AAS 15-330

ORBITAL PERTURBATION ANALYSIS NEAR BINARY ASTEROID SYSTEMS

Loic Chappaz,[*] Stephen B. Broschart,[†] Gregory Lantoine,[†] and Kathleen Howell[‡]

Current estimates indicate that approximately sixteen percent of the known near-Earth asteroid population may be binaries. Within the context of exploring the dynamical behavior of a spacecraft orbiting or moving near such systems, a first step in the analysis is an assessment of the perturbing effect that dominates the dynamics of the spacecraft. The relative strength of several perturbations, including the perturbation that arises from the existence of a binary system, rather than a single body system, is compared by exploiting 'zonal maps'. Such a map is useful in determining the type of orbit that is practical in support of a given mission scenario.

INTRODUCTION

Small bodies are the focus of increasing scientific interest and their study offers insight into the early development of the solar system, as well as the formation and origin of more massive bodies. However, ground-based observations possess limited capabilities and closer observations, available during in situ missions, supply higher volume and higher quality data for analysis. In recent years, several spacecraft have been delivered to the vicinity of small irregular bodies and more complex missions are under development. Currently, ESA's Rosetta spacecraft is orbiting comet 67P/ChuryumovGerasimenko and has successfully delivered a lander to the comet's surface.[1] In 2016, the NASA mission OSIRIS-REX is scheduled to deliver a spacecraft to the asteroid 1999 RQ36 to collect soil samples and to investigate this potentially hazardous object.[2] Based upon such initial steps, the number of proposals involving such spacecraft destinations is generally increasing. In addition, current estimates indicate that approximately sixteen percent of the known near-Earth asteroid population may be binaries[3] and a few new mission concepts are emerging to visit binary systems comprised of irregular bodies. The ESA-led MarcoPolo-R mission was initially proposed to visit a near-Earth binary asteroid[4] and a NASA AMES investigation proposed a future mission scenario to explore the binary system Didymos.[5] The Asteroid Impact and Deflection Assessment (AIDA) is another mission scenario currently under development conjointly at NASA and ESA whose target is the binary asteroid Didymos. This scenario aims to demonstrate the kinetic impactor concept to deflect an asteroid by impacting the secondary component of the binary sys-

[*]Ph.D Candidate, School of Aeronautics and Astronautics, Purdue University, 701 W Stadium Ave., West Lafayette, IN 47906; Member AAS, AIAA.

[†]Mission Design Engineer, Mission Design and Navigation Section, Jet Propulsion Laboratory, California Institute of Technology, 4800 Oak Grove Dr., Pasadena, CA 91109.

[‡]Hsu Lo Distinguished Professor, School of Aeronautics and Astronautics, Purdue University, 701 W Stadium Ave., West Lafayette, IN 47906; Fellow AAS, AIAA.

tem.[6] With other complex plans emerging, further exploration of the dynamical behavior in such an environment is warranted.

Within the context of exploring the dynamical behavior of a spacecraft near a pair of small irregular bodies, a first step in the analysis is an assessment of the perturbing effect that dominates the dynamics of the spacecraft in such a region as a function of the baseline orbit. Previous investigators examined this problem for a single body, e.g., an asteroid,[7] a comet,[8] or a planet,[9] as well as considering the perturbations from the solar tide, Solar Radiation Pressure (SRP), and the small body oblateness. The objective in this investigation is an extension of the analysis to include the perturbation that arises from the existence of the secondary body in a binary system. To compare the relative strength of several perturbing effects across the parameter space, 'zonal maps' are introduced. Then, the prediction of the binary effect is initially validated using arbitrary initial conditions that are numerically propagated in the circular restricted three-body problem. The validity of the zonal map is further assessed through the numerical integration of initial conditions, that correspond to pre-computed periodic orbits, with a high-fidelity dynamical model.

DYNAMICAL MODELS

Conic Restricted Four-Body Problem (CR4BP) and Augmented CR4BP (ACR4BP)

In scenarios that involve the close proximity of a spacecraft to a pair of small bodies, it may not be reasonable, in general, to represent the system of small bodies as a single mass distribution. Spacecraft trajectories are often designed leveraging simplified dynamical models. However, these models are an idealized representation of the dynamics, and a spacecraft trajectory that is constructed with such representations requires validation in a higher-fidelity model to assess the suitability of such a solution in actual mission scenarios. Consider a model that incorporates the gravitational attraction of the Sun and both components of the binary system. It is assumed that the secondary component in the binary system, P_2, evolves in a conic orbit with respect to the primary, P_1. Similarly, it is also assumed that the binary system is traveling along a conic orbit around the Sun centered at the binary barycenter. These two conic orbits can be fully described by the set of classical orbital elements $\bar{oe}_{P_2}$ and $\bar{oe}_{Sun}$ for P_2 and the Sun, respectively. Additionally, each component of the binary is modeled as a constant density polyhedron and the gravitational attraction that is associated with each body is computed consistent with its shape model. Such a model is labeled the Conic Restricted Four-Body Problem (CR4BP) in this analysis. Finally, in the Augmented CR4BP (ACR4BP), the solar radiation pressure that is exerted onto the spacecraft is also incorporated into the dynamical model. In this analysis, a simple model that assumes the spacecraft is spherical and possesses a constant reflectivity is employed to include this perturbing effect. Then, as expressed in an inertially fixed frame centered at the primary P_1, the equations of motion for a spacecraft in the ACR4BP are written as,

$$\ddot{\bar{\rho}} = \frac{\partial U_{P_1}}{\partial \bar{\rho}} + \frac{\partial U_{P_2}(\bar{\rho}_{s/c\to P_2})}{\partial \bar{\rho}_{s/c\to P_2}} + \frac{\partial U_{Sun}(\bar{\rho}_{s/c\to Sun})}{\partial \bar{\rho}_{s/c\to Sun}} + \bar{a}_{SRP} \tag{1}$$

where $\bar{\rho}$, $\bar{r}_{P_2}$, $\bar{r}_{Sun}$ denote the nondimensional position vector with respect to P_1 of the spacecraft, P_2, and the Sun, respectively. Then, $\bar{\rho}_{s/c\to P_2} = \bar{\rho} - \bar{r}_{P_2}$, $\bar{\rho}_{s/c\to Sun} = \bar{\rho} - \bar{r}_{Sun}$. Also, the symbols U_{body} represent the gravitational potential function that is associated with the body in the subscript expression and $\bar{a}_{SRP}$ is the solar radiation pressure acceleration.

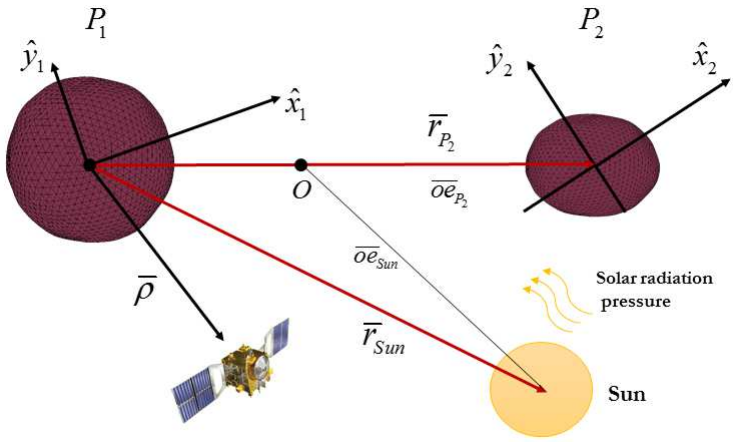

Figure 1. ACR4BP geometry

Circular Restricted Three-Body Problem (CR3BP)

The CR3BP is a simplified dynamical model that is useful to design trajectories assuming this model supplies a reasonable approximation for the dynamical regime near systems of small bodies. Consider a model that incorporates two massive bodies and relies on simplifying assumptions. In the CR3BP, the two primaries are point masses, labeled P_1 and P_2 with masses m_1 and m_2, respectively. The mass parameter of the system is defined as $\mu = \frac{m_2}{m_1+m_2}$ and the orbits of the two bodies are assumed to be coplanar and circular relative to the system barycenter. A barycentric rotating frame is defined such that the $\hat{z}$-axis is aligned with the angular velocity of the primary system, the $\hat{x}$-axis is directed from P_1 to P_2, and the $\hat{y}$-axis completes the right-handed basis. The nondimensional equations of motion for a third-body in the CR3BP, as expressed in the rotating frame, are reduced to,

$$\ddot{\bar{\rho}} = [2n\dot{y} + U_x, -2n\dot{x} + U_y, U_z] \tag{2}$$

where n is constant and equal to 1 in the nondimensional unit system and $\bar{\rho} = x\hat{x} + y\hat{y} + z\hat{z}$ denotes the location of the third body in the rotating frame with respect to the primary system barycenter. Then, $U(x, y, z, n) = \frac{1}{2}n^2\left(x^2 + y^2\right) + \frac{1-\mu}{d} + \frac{\mu}{r}$ is the pseudo-potential function, d and r represent the distances between the third body and the primaries P_1 and P_2, respectively. Then, the quantities U_x, U_y, and U_z represent the partial derivatives of U with respect to the nondimensional coordinates of the third body position. The EOMs are time-invariant and there is a unique known integral of the motion, labeled Jacobi constant, defined as $C = 2U - v^2$ where v denotes the magnitude of the rotating velocity vector of the third body.

ORBITAL PERTURBATIONS

To initially assess the perturbing effects that drive the behavior of the spacecraft, the Lagrange Planetary Equations (LPE) are exploited. First, assume that the reference or baseline trajectory of the spacecraft is an orbit about P_1. Then, to model the perturbation on a spacecraft that is associated with the existence of a secondary body in the primary system, labeled 'binary effect' in this analysis, the three-body disturbing function is exploited.[10] This function is derived as an infinite

series expansion in terms of the orbital elements of both of the additional masses, i.e., the spacecraft and the secondary, each moving with respect to a central body, i.e., the primary P_1. In this analysis, the investigation is limited to the secular effects. To second order in inclination and eccentricities, the averaged secular term in the disturbing function simplifies to a reasonably tractable expression and allows an approximation for the disturbing potential that corresponds to the binary effect.

Lagrange Planetary Equations (LPE)

The LPEs supply approximate equations of motion in terms of the classical orbital elements for the secular time evolution of the elements due to a specific perturbing effect. The LPEs rely on the availability of a scalar perturbing potential function, R, that represents the perturbing effect. Let $\bar{oe} = [a, e, i, \omega, \Omega, \sigma]$ denotes the classical set of orbital elements for the spacecraft in the inertial frame and n is the mean motion of the spacecraft. These equations are written as,[10]

$$\dot{a} = \frac{2}{na}\frac{\partial R}{\partial \sigma} \tag{3}$$

$$\dot{e} = \frac{1}{na^2 e}\left[\left(1-e^2\right)\frac{\partial R}{\partial \sigma} - \sqrt{1-e^2}\frac{\partial R}{\partial \omega}\right] \tag{4}$$

$$\dot{i} = \frac{1}{na^2\sqrt{1-e^2}}\left[\cot i\frac{\partial R}{\partial \omega} - \csc i\frac{\partial R}{\partial \Omega}\right] \tag{5}$$

$$\dot{\omega} = \frac{\sqrt{1-e^2}}{na^2 e}\frac{\partial R}{\partial e} - \frac{\cot i}{na^2\sqrt{1-e^2}}\frac{\partial R}{\partial i} \tag{6}$$

$$\dot{\Omega} = \frac{\csc i}{na^2\sqrt{1-e^2}}\frac{\partial R}{\partial i} \tag{7}$$

$$\dot{\sigma} = -\frac{1-e^2}{na^2 e}\frac{\partial R}{\partial e} - \frac{2}{na}\frac{\partial R}{\partial a} \tag{8}$$

One challenge in analyses that involve the use of the LPEs, besides the availability of a closed-form expression for the perturbing potential function, is an expression of this function in terms of the orbital elements. Such a form is required to compute the partial derivatives of the potential with respect to the orbital elements.

Classical Perturbing Effects

The classical perturbing effects that are considered in problems that involve single bodies, the main focus of previous developments, include the SRP,[7] solar tide,[11] and body oblateness.[7] For these effects, potential functions that describe the perturbing effect can be derived and substituted into the LPEs. While these equations provide an approximation for the secular evolution of the orbital elements due to any given effect, the objective is to assess the relative strength of the various perturbations. Then, as discussed in Scheeres,[7] one approach to quantify the strength of a perturbation relies on identifying common coefficients in the LPEs, for a given effect. Such a coefficient is a measure of the strength of a perturbation. These coefficients are derived as,[7]

$$C_t = \frac{\dot{N}^2}{n} \tag{9}$$

$$C_g = \frac{3gna^2}{2\mu_{pb}} \tag{10}$$

$$C_s = \frac{3nJ_2\alpha_0^2}{2a^2} \tag{11}$$

for the solar tide, the SRP, and the body oblateness, respectively. The symbols N and n denote the mean motion of the small body and spacecraft in their orbits relative to the Sun, respectively. Then, in the expression for C_g, g denotes the SRP force and is defined as $g = G_1 B/R^2$, where G_1 is the solar flux constant ($\approx 1 \times 10^{14}$ kgkm/s^2), B is the effective projected area-to-mass ratio of the spacecraft, and μ_{pb} is the gravitational parameter of the small body. Also, the symbol J_2 describes the oblateness of the primitive body and α_0 is the largest equatorial radius of the body.

Third-Body Disturbing Function

The objective is to extend the analysis to include the perturbation that corresponds to the existence of a secondary component rather than a single central body. To model this perturbation, labeled 'binary effect' in this analysis, the three-body disturbing function is exploited.[10] This function is derived as an infinite series expansion in terms of the orbital elements of the two additional masses, the secondary and the spacecraft, with respect to a central body, as illustrated in Figure 2. The disturbing function is derived in details in Murray and Dermott[10] and the application of this theory to the problem of interest in this investigation is briefly outlined in this section. Most often, the disturbing function is written as the sum of two parts, the direct and indirect term. In this analysis, the investigation is limited to the secular effects from the secondary. Considering only secular effects, the indirect term vanishes and only the direct part is relevant. Also, note that the form of the perturbing potential depends on the relative location of the spacecraft and secondary. When the spacecraft orbit lies outside of the secondary orbit with respect to the primary, the secondary is then an internal perturber. The perturbing function differs if it is due to an external perturber, when the spacecraft orbit is contained inside the orbit of the secondary with respect to the primary. It is further assumed that the orbits of the secondary and the spacecraft never intersect. Then, the perturbing functions R_1 and R_2 for an external and internal perturber, respectively, are expressed as,

$$R_1 = \frac{Gm_2}{a_2} R_d^{<sec>} = \frac{Gm_2}{a_1} \alpha_{12} R_d^{<sec>} \tag{12}$$

$$R_2 = \frac{Gm_1}{a_1} \alpha_{12} R_d^{<sec>} = \frac{Gm_1}{a_2} R_d^{<sec>} \tag{13}$$

where G is the universal gravitational constant, the subscripts $1, 2$ correspond to quantities that are associated with the perturber and perturbed body, respectively. Then, α_{12} is defined as the ratio a_2/a_1 and $R_d^{<sec>}$ is the averaged secular direct term of the disturbing function. In this analysis, the focus is the perturbation on the spacecraft that arises from the secondary,P_2, thus, the two relationships can be reduced to a single equation such that,

$$R_i = \frac{Gm_2}{a}\bar{\alpha}R_d^{<sec>}, i = 1, 2 \tag{14}$$

where $\bar{\alpha}$ is defined as,

$$\bar{\alpha} = \begin{cases} \alpha & \text{if } i = 1, \\ 1 & \text{if } i = 2. \end{cases} \tag{15}$$

and $\alpha = \alpha_{12}$ for clarity. To second order in inclination and eccentricities, the averaged direct term in the disturbing function, that is, the terms that correspond to secular effects, can be written as,

$$\begin{aligned} R_D^{<sec>} = \frac{1}{8}\alpha b_{3/2}^{(1)}\left(e^2 + e_2^2\right) - \frac{1}{2}\alpha b_{3/2}^{(1)}\left(s^2 + s_2^2\right) \\ -\frac{1}{4}\alpha b_{3/2}^{(2)} e e_2 \cos\left(\omega - \omega_2\right) + \alpha b_{3/2}^{(1)} s s_2 \cos\left(\Omega - \Omega_2\right) \end{aligned} \tag{16}$$

where $s = \sin\left(\frac{1}{2}i\right)$, and the subscript 2 now refers to the orbital elements that are associated with the secondary body, P_2. Then, the Laplace coefficient $b_s^{(j)}$ is defined as,

$$b_s^{(j)}(\alpha) = \frac{1}{2\pi}\int_0^{2\pi} \frac{\cos j\psi \mathrm{d}\psi}{(1 - 2\alpha\cos\psi + \alpha^2)^s} \tag{17}$$

Substituting Eqs. (16) and (17) into Eq. (14) provides an expression for the perturbing potential that arises from the existence of a secondary as a function of the classical orbital elements of the spacecraft.

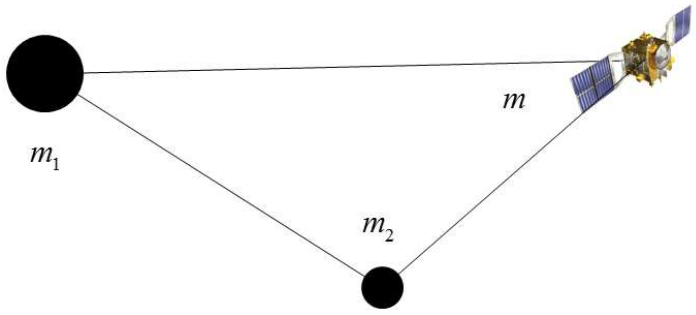

Figure 2. Problem geometry

Binary Effect

To construct the LPEs that correspond to the binary effect, the disturbing function, R_i, derived in Eq. (14) is employed as the perturbing potential, R. Then, the partial derivatives of R_i with respect to the classical set of orbital elements are required. However, the perturbing potential is averaged, hence, the LPE that is associated with the secular evolution of the true anomaly, σ is discarded.

Consequently, the partial derivative of the perturbing potential with respect to the semi-major axis, a, is not required and the partial with respect to σ is set to equal to zero. Also recall that the disturbing function is expressed in terms of the variables s, s_2, rather than directly in terms of the inclinations i, i_2, where $s = \sin\left(\frac{1}{2}i\right)$. Thus, the following partial derivatives are required for the derivation,

$$\frac{\partial s}{\partial i} = \frac{1}{2}\cos\left(\frac{1}{2}i\right) \tag{18}$$

$$\frac{\partial s^2}{\partial i} = \cos\left(\frac{1}{2}i\right)\sin\left(\frac{1}{2}i\right) = \frac{1}{2}\sin i \tag{19}$$

The remaining partial derivatives are derived as,

$$\frac{\partial R_D^{<sec>}}{\partial e} = \frac{1}{4}\alpha b_{3/2}^{(1)} e_2 - \frac{1}{4}\alpha b_{3/2}^{(2)} e\cos\left(\omega - \omega_2\right) \tag{20}$$

$$\frac{\partial R_D^{<sec>}}{\partial i} = -\frac{1}{4}\alpha b_{3/2}^{(1)} i_2 + \frac{1}{2}\alpha b_{3/2}^{(1)} s_2\cos\left(\frac{1}{2}i\right)\cos\left(\Omega - \Omega_2\right) \tag{21}$$

$$\frac{\partial R_D^{<sec>}}{\partial \omega} = \frac{1}{4}\alpha b_{3/2}^{(2)} e e_2\sin\left(\omega - \omega_2\right) \tag{22}$$

$$\frac{\partial R_D^{<sec>}}{\partial \Omega} = -\alpha b_{3/2}^{(1)} s s_2\sin\left(\Omega - \Omega_2\right) \tag{23}$$

Assuming the orbit of the secondary with respect to the primary is planar and circular, i.e., $e_2 = i_2 = 0$, the partial derivatives reduce to,

$$\frac{\partial R_D^{<sec>}}{\partial e} = \frac{1}{4}\alpha b_{3/2}^{(1)} e \tag{24}$$

$$\frac{\partial R_D^{<sec>}}{\partial i} = -\frac{1}{4}\alpha b_{3/2}^{(1)} i \tag{25}$$

$$\frac{\partial R_D^{<sec>}}{\partial \omega} = 0 \tag{26}$$

$$\frac{\partial R_D^{<sec>}}{\partial \Omega} = 0 \tag{27}$$

Note that the inclination assumption can be made without loss of generality by defining the elements with respect to the binary orbit plane. Then, recall the definition of the perturbing potential for the perturbation of interest,

$$R = R_i = \frac{Gm_2}{a}\bar{\alpha} R_d^{<sec>}, i = 1, 2 \tag{28}$$

Thus, the partial derivatives with respect to the set of orbital elements, oe,

$$\frac{\partial R}{\partial oe} = \frac{Gm_2}{a}\bar{\alpha}\frac{\partial R_D^{<sec>}}{\partial oe} \tag{29}$$

and substituting $\frac{\partial R}{\partial oe}$ in the LPEs in Eq. 3,

$$\dot{a} = 0 \tag{30}$$

$$\dot{e} = 0 \tag{31}$$

$$\dot{i} = 0 \tag{32}$$

$$\dot{\omega} = \frac{\mu_2}{4na^3}\alpha\bar{\alpha}b_{3/2}^{(1)}\left\{\sqrt{1-e^2} + \frac{\cos i}{\sqrt{1-e^2}}\right\} \tag{33}$$

$$\dot{\Omega} = \frac{-\mu_2}{4na^3}\alpha\bar{\alpha}b_{3/2}^{(1)}\frac{1}{\sqrt{1-e^2}} \tag{34}$$

Hence, define C_b the strength coefficient for the 'binary effect' as,

$$C_b = \frac{\mu_2}{4na^3}\alpha\bar{\alpha}b_{3/2}^{(1)} \tag{35}$$

where C_b is selected as the common factor in the two non-zero LPEs in Eqs. (30)-(34).

Eccentricity Terms

In the current expressions for the strength coefficients, note that there is no dependence on eccentricity. However, some commonality in terms of eccentricity exists in the LPEs that are associated with a given effect.[7,11] Including the common eccentricity terms into the strength coefficients allows the derivation of an augmented set of coefficients that are now eccentricity dependent,

$$C_t' = \frac{\dot{N}^2}{n}\frac{1}{(1-e^2)^{1/2}} \tag{36}$$

$$C_g' = \frac{3gna^2}{2\mu_{pb}} \tag{37}$$

$$C_s' = \frac{3nJ_2\alpha_0^2}{2a^2}\frac{1}{(1-e^2)^{3/2}} \tag{38}$$

$$C_b' = \frac{\mu_2}{4na^3(1-e^2)^{1/2}}\alpha\bar{\alpha}b_{3/2}^{(1)} \tag{39}$$

Note that the SRP coefficient remains unchanged as the LPE that corresponds to the eccentricity evolution is non-zero. Thus, the eccentricity does not remain constant, on average, and it is not reasonable to include eccentricity in the strength coefficient. Such a coefficient only includes constant quantities, on average.

Binary Effect Initial Validation

The LPEs applied to the binary effect supply an approximation for the secular evolution of the orbital elements of a spacecraft orbit assuming the binary effect is the only perturbation considered. To assess the relevance of the binary effect strength coefficient, the prediction of the binary effect is initially validated using arbitrary initial conditions that are numerically propagated in the Circular

Restricted Three-Body Problem. Then, consistent with the LPE derived in Eqs. (30)-(34), the semi-major axis, eccentricity, and inclination are to remain constant, on average, while the argument of periapsis and the longitude of the right ascending node may vary linearly such that,

$$\omega(t) = C_b' \left(1 - e^2 + \cos i\right) t + \omega_0 \tag{40}$$

$$\Omega(t) = C_b' t + \Omega_0 \tag{41}$$

The initial conditions are numerically propagated for 10 revolutions and the corresponding paths, as computed both in the two-body problem and CR3BP, are illustrated in black and blue, respectively, in Figure 3. In the left and right plot, the paths are displayed as viewed in the inertial frame and synodic frame, respectively. The correspond osculating orbital elements for the 3BP trajectory are represented in Figure 4.

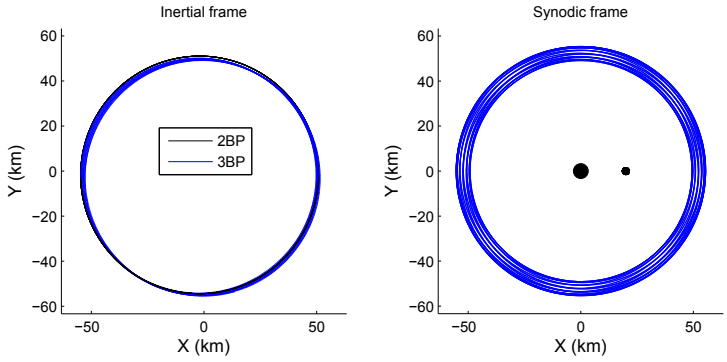

Figure 3. Conic orbit propagation with the 2BP and CR3BP.

While the two-body trajectory is a closed conic, one that retraces the same path over the revolutions, it is clear that the 3BP trajectory is no longer Keplerian, as a result of the presence of a secondary massive body. In the right plot, the same 3BP trajectory as viewed in the synodic frame further emphasizes the non-Keplerian nature of the path. Then, it is apparent from the osculating orbital elements representation that the semi-major axis, eccentricity, and inclination remain constant, on average, consistent with the LPE prediction. Also, the predictions for the secular variation of the two non-zero LPE, corresponding to the argument of periapsis and the longitude of the right ascending node, are overlaid on the corresponding figures in red. Clearly, the prediction captures the average secular evolution of the two orbital elements. This simple scenario provides an initial validation for the derived LPEs that correspond to the binary effect and, thus, also supplies some insight supporting the validity of the binary strength coefficient.

ZONAL MAPS

To compare the relative strength of several perturbing effects across the parameter space, 'zonal maps' are introduced, or, a two-dimensional representation similar to an exclusion plot.[12] A zonal map depicts the dominating perturbing effect as a function of the spacecraft orbit semi-major axis with respect to the primary, the eccentricity, and the mass ratio of the binary system, where the mass ratio is defined as the mass of the secondary to the total mass of the system. Note that these

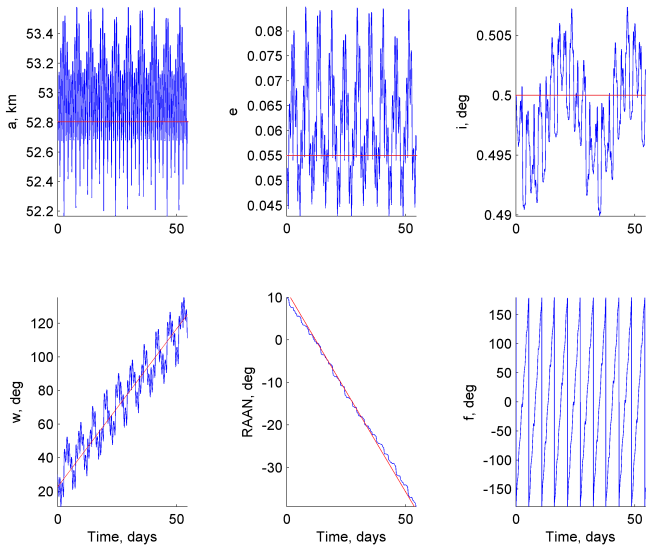

Figure 4. Orbital elements for CR3BP trajectory, red straight line is the LPE prediction.

zones are also strongly dependent on the J_2 coefficient and β, the non-dimensional acceleration due to SRP, assuming a spherical spacecraft. For a sample binary system model, a zonal map that is generated following the proposed strategy is illustrated in Figure 5 with $\beta = 5$, $J_2 \approx 0.057$, and $e = 0.05$. Colored in shades of blue, red, and green, the corresponding regions are dominated by the oblateness of the body, the binary effect, and the SRP, respectively. Note that the spacecraft semi-major axis is scaled by the primary separation distance; thus, a value of one corresponds to the location of the secondary. Also, filled contours labeled '10' and '100' correspond to regions where the dominating perturbation is stronger than any other effect in excess by the corresponding factor, labeled Maximum Strength Coefficient Ratio (MSCR).

In general, the binary effect dominates for values of the semi-major axis close to the secondary location. Also, as the mass ratio increases, that is, the mass of the secondary relative to the primary increases, the binary effect is stronger, as expected. Then, the primary oblateness perturbation dominates for the smallest semi-major axis values, and may also dominate over the binary effect for the smallest mass ratios. As semi-major axis values increase, the strongest perturbation is the SRP. Finally, while the perturbation from the solar tide is also incorporated into the analysis, this effect never dominates the other perturbations over the range of semi-major axes that are investigated.

The zonal maps are useful in determining the type of orbit that is practical to support a given mission scenario. For instance, for a scenario that involves close spacecraft proximity to either body, three-body trajectories are relevant, e.g., Distant Retrograde Orbits (DRO), Low Prograde Orbits (LoPO), and Halo orbits.[13] However, for a scenario such that the spacecraft orbit evolves further away from the primary system, trajectories that are driven by SRP are most useful, e.g., terminator orbits.[14] Within that context, information regarding sample types of periodic orbits is overlaid on the zonal map. For terminators, the range for the mean semi-major axis with respect to P_1 for the terminator family that corresponds to the β value in the map is represented by the blue line. For the P_1 centered LoPO and DRO families, since these orbits are constructed in a three-body

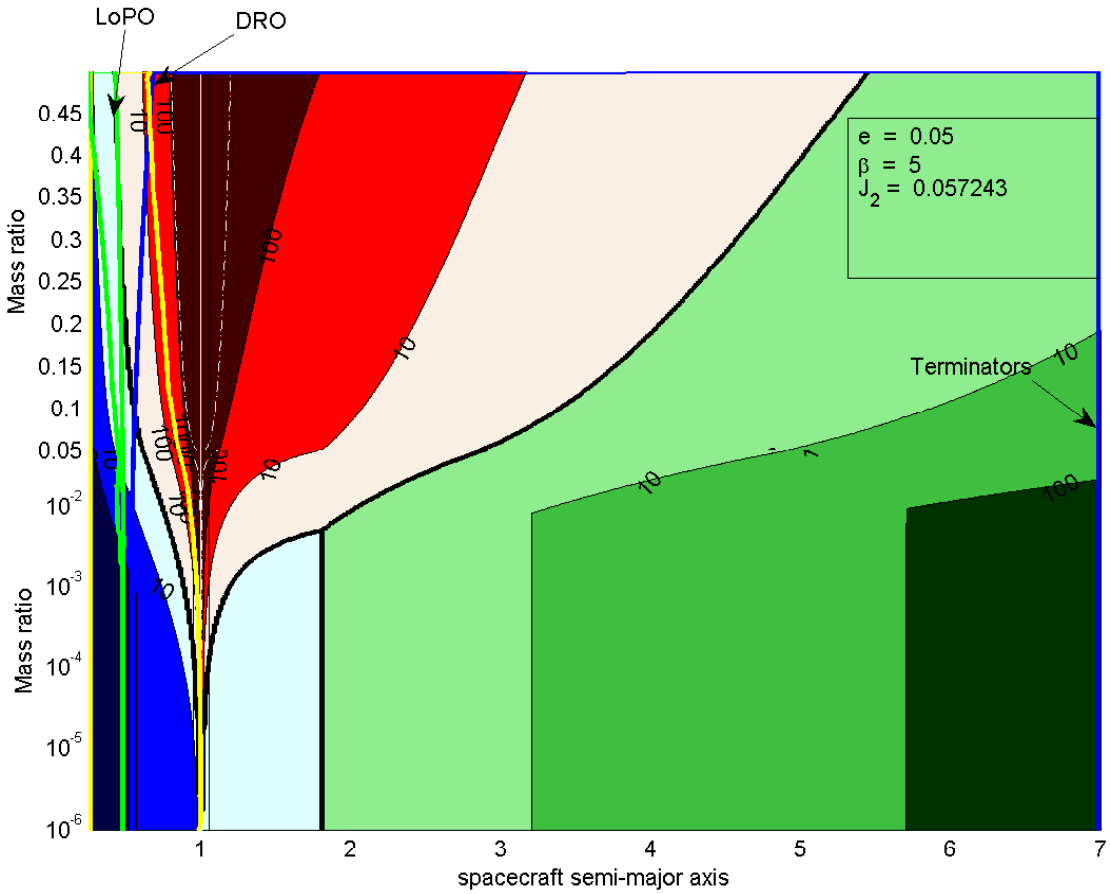

Figure 5. Zonal Map: semi-major axis against mass ratio. Blue: J_2 dominated, red: binary effect dominated, green: SRP dominated

model, the closest approach with respect to P_1 is employed as a proxy for the semi-major axis and reported on the zonal map with the green and yellow lines.

The zonal maps can incorporate other axes as well. In Figure 6(a), a similar map is illustrated in terms of spacecraft semi-major axis against eccentricity for a mass ratio equal to 0.05. Finally, a map depicting the same zones now in terms of spacecraft eccentricity against mass ratio appears in Figure 6(b) for $a = 2.5$. Depending on the type of spacecraft orbits or motion that is relevant to a particular analysis, the set of axes most suited to yield insight for the trajectory design process may vary.

APPLICATION TO PERIODIC ORBIT STABILITY

The validity of the zonal map is further assessed through the numerical integration of initial conditions that correspond to pre-computed periodic orbits with a higher-fidelity dynamical model. The higher-fidelity model incorporates the various perturbing effects and the stability of periodic orbits that are initially computed in a simplified dynamical model is explored. Different types of families are considered: families that are constructed exploiting the three-body regime as well as orbits that rely on SRP, i.e. terminator orbits.

Periodic Orbits Stability

A key factor to assess the suitability of a trajectory for a given application is often its stability. Significant information concerning the stability of a particular solution is available from the first-order variational equations relative to a reference. For a periodic orbit, the monodromy matrix, M, is defined as the state transition matrix evaluated after exactly one orbital revolution along the reference path, that is, $M = \Phi(t + P, t)$. The eigenvalues of the monodromy matrix are then computed for each orbit of interest. The dynamical model for the motion of a particle in this problem represents a three degree-of-freedom Hamiltonian system. Consequently, the monodromy matrix admits six eigenvalues that occur in reciprocal pairs,[15] where two are always equal to unity.[16] If all eigenvalues possess magnitudes less than 1, the orbit is defined as stable, and alternatively, an orbit is labeled unstable if any eigenvalue has a magnitude greater than 1.

Periodic Orbits of Interest

To explore the dynamical behavior of a third body within the vicinity of two primaries, periodic orbits are of special interest. A multi-phase technique based on differential corrections is employed to compute a trajectory that is periodic in the nonlinear regime given some initial guess. A trajectory is labeled periodic if the discontinuity between the initial and final six-dimensional states along the path does not exceed a prescribed tolerance, typically 10^{-11} nondimensional units.

Libration Point periodic Orbits. (LPO) Many families of periodic orbits within the three-body regime are associated with the equilibrium points and, thus, are labeled libration point orbits. A preliminary exploration of the dynamical structures typically originates near any equilibrium solutions. The first-order variational equations of motion are employed to generate an initial guess in the vicinity of a given equilibrium point. In this problem, there are, in general, five equilibrium points and the equilibrium locations evolve as a function of the system mass ratio. First, the planar Lyapunov families corresponding to the collinear Lagrange points are computed for a sample system. Employing a continuation strategy, additional families of more complex orbits that include three-dimensional trajectories are also computed. In particular, L_1 and L_2 halo orbits are examples

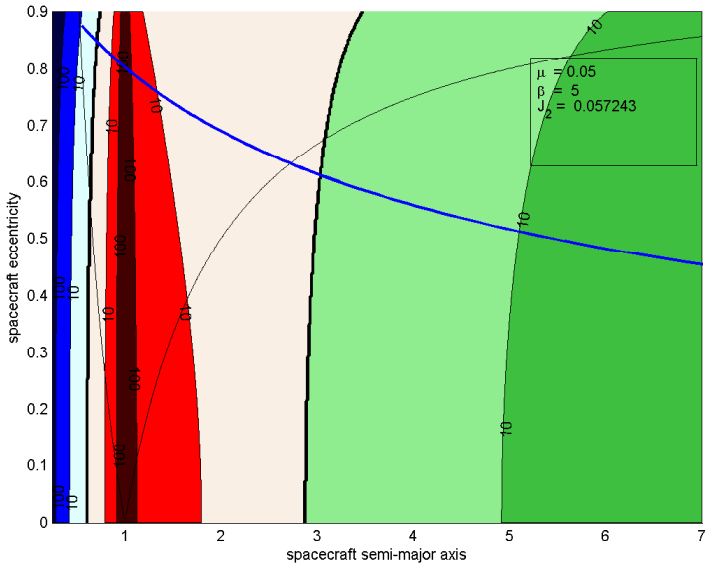

(a) Zonal map: semi-major axis against eccentricity

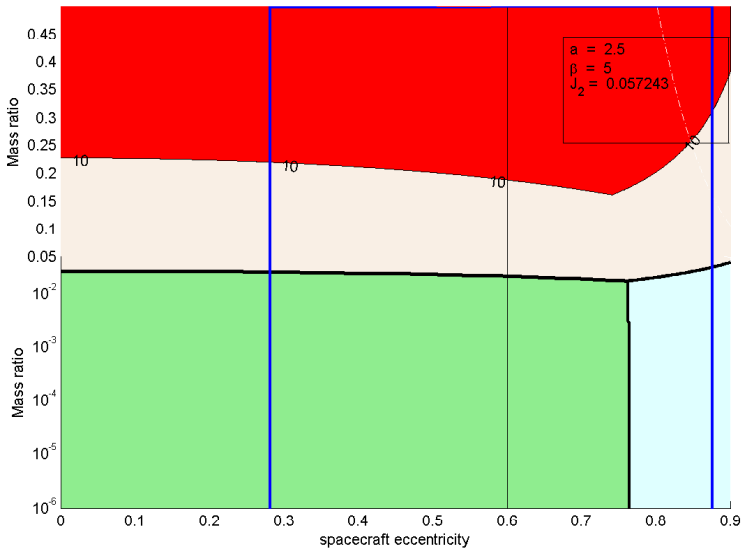

(b) Zonal map: eccentricity against mass ratio

Figure 6. Zonal maps including eccentricity information. Blue: J_2 dominated, red: binary effect dominated, green: SRP dominated

of families that possess a geometry that is especially interesting to observe one of the primaries and also feature some stable members, as illustrated in Figure 7 for a mass ratio equal to 0.1. The individual trajectories are colored in blue and red for stable and unstable orbits, respectively.

Terminator Orbits Terminator orbits are one of the few types of ballistic orbits known to exhibit stable and robust motion in the presence of strong solar radiation pressure.[7] Also, the robust stability

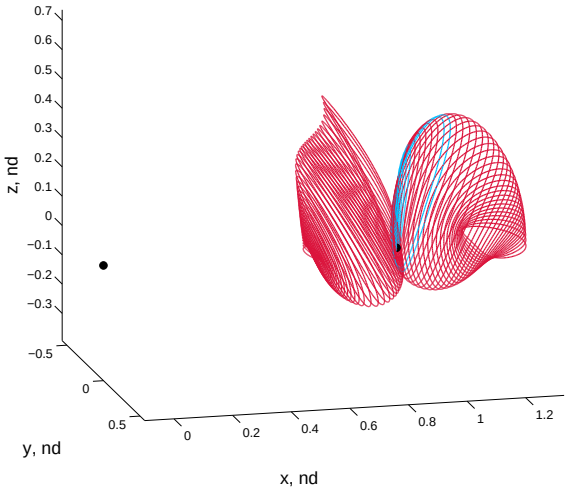

Figure 7. L_1 **and** L_2 **halo families: mass ratio** $\mu = 0.1$

characteristics of terminator orbits extend to long-term stable motion in the presence of an irregular gravitational field.[14] In scenarios such that stable orbital dynamics are desired, such properties suggest terminator orbits as ideal candidates for orbiting a small irregular body. Terminator orbits are oriented such that the orbital plane is approximately normal to the SRP acceleration through any time evolution, that is, the angular momentum vector for terminator orbits is parallel to the direction of the Sun. In this analysis, the robustness of such orbits is assessed by including a secondary massive body in the primary system. Terminator orbits are initially computed in the Augmented Hill Three-Body Problem and parameterized by the SRP nondimensional acceleration coefficient, β.[17] In Figure 8 are illustrated two families of such terminator orbits for β values equal to 1000 and 1; the larger the β value, the stronger the SRP acceleration relative to gravitational forces. The members in each family are repented in blue and red for stable and unstable orbits, respectively.

Low Prograde Orbits (LoPO) and Distant Retrograde Orbits (DRO) Periodic orbits labeled Distant Retrograde Orbits (DRO) and Low Prograde Orbits (LoPO) are also of special interest as these families feature numerous stable orbits. The DROs are, in fact, 1:1 resonant orbits. The classical restricted two-body problem is leveraged to generate an initial guess to produce a periodic orbit in the three-body regime via a corrections strategy and/or continuation. A sample family for a mass ratio equal to 0.2 is illustrated in Figure 9 where the individual trajectories are colored in blue and red for stable and unstable orbits, respectively. It is, then, clear that the DRO family features numerous stable orbits. Planar LoPOs are also centered at one primary, P_1 or P_2. Exploiting bifurcations within the planar families, and employing a continuation technique, a three-dimensional family that branches from the planar family is also computed, as illustrated in Figure 10 for a sample system with a mass ratio equal to 0.2. As clearly apparent in the figure, the orbits in the three-dimensional families allow regular close-range proximity of a third-body with respect to either primary. In addition, the three-dimensional aspect of the trajectories offers extensive coverage of the surface of the attractive primary.

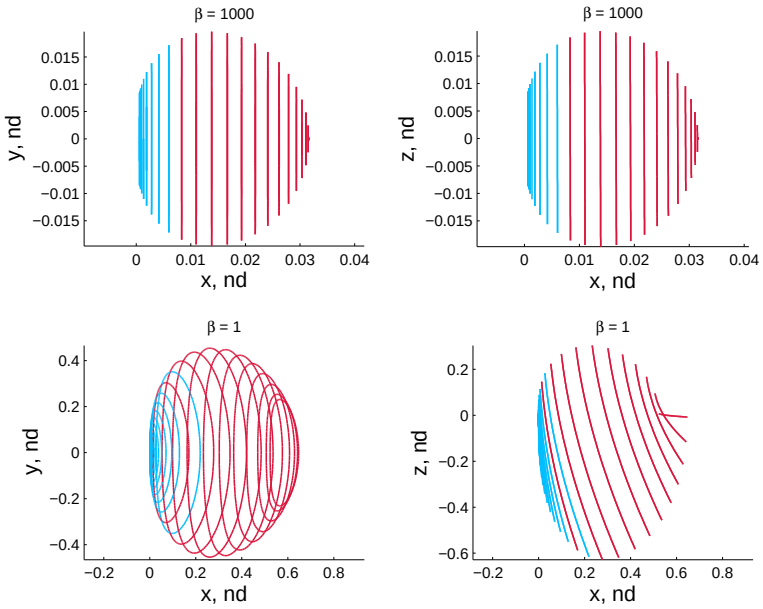

Figure 8. Terminator families for $\beta = 1000$ (top) and $\beta = 1$ (bottom).

Application to Sample Orbits

Binary effect regime: L_2 halo orbit The existence of halo orbits relies on the presence of a secondary massive body in the primary system, thus, such orbits are characteristic of a binary effect dominated regime. Although some stable orbits exist for most mass ratios, these orbits are only 'weakly stable'. Consider a sample stable L_2 halo orbit for a mass ratio approximately equal to 0.0034. First, the initial conditions that are associated with this orbit are propagated in a higher-fidelity model that includes the solar tide (CR4BP) and an oblate P_2. The resulting trajectory is plotted in Figure 11(a) and appears to remain bounded and stable for 10 revolutions. However, repeating the same simulation, now also including the SRP (ACR4BP), the trajectory only remains bounded for 3 revolutions before escaping the vicinity of P_2, even though the MSCR (ratio of the dominating perturbation strength coefficient to the second stronger) is approximately equal to 20. While defined as linearly stable, halo orbits, in general, are quite sensitive to pertubations and may not be ideal candidates for long-term stable ballistic motion.

Binary effect regime: DRO The DROs are another example of an orbit that only exists when the primary system is comprised of two massive bodies. However, in contrast to halo orbits, numerous stable and robust orbits for all mass ratios exist. To demonstrate these properties, a sample DRO for a mass ratio equal to 0.4 and a closest P_1 approach corresponding to a binary effect dominated regime with a MSCR approximately equal to 25 is numerically propagated in the ACR4BP. In this scenario, The higher-fidelity model now includes the SRP acceleration, irregular shape models for the primaries, and the solar tide. Further, to also assess the out-of-plane stability of such an orbit, a initial out-of-plane velocity perturbation is introduced. The resulting trajectory is illustrated in Figure 12 and, while the path appears to be disturbed by the various perturbing effects introduced, the trajectory remains bounded and in the vicinity of the nominal DRO for 10 revolutions.

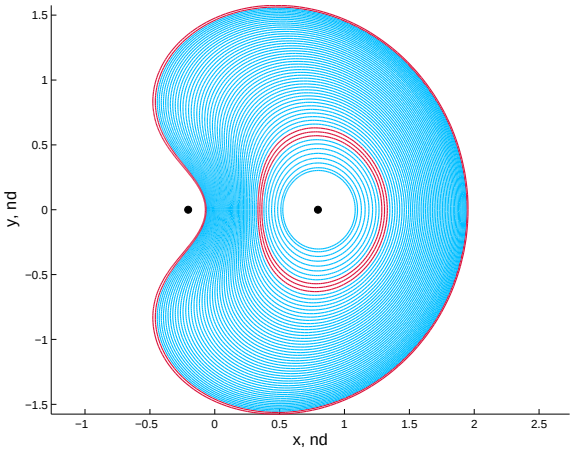

Figure 9. DRO family: mass ratio $\mu = 0.2$

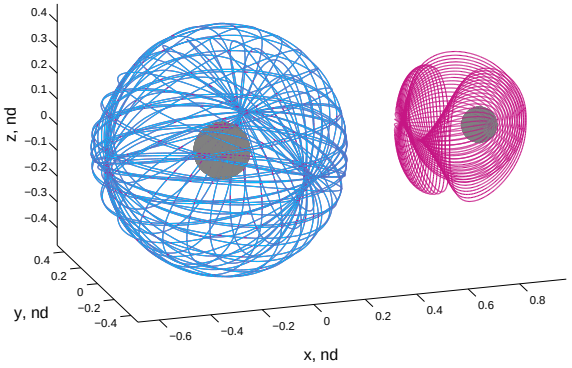

Figure 10. P_1 and P_2 centered 3D LoPO families: mass ratio $\mu = 0.2$

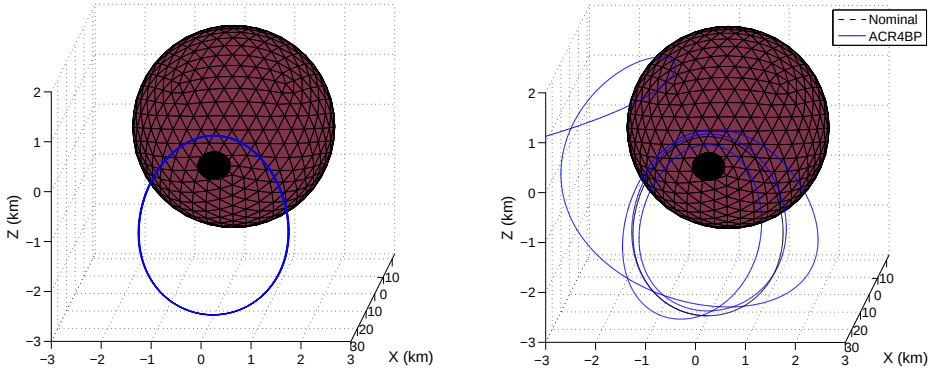

(a) CR4BP with oblate secondary (b) ACR4BP with oblate secondary

Figure 11. Sample stable L_2 halo orbit propagated in higher-fidelity dynamical model: mass ratio $\mu = 0.0034$

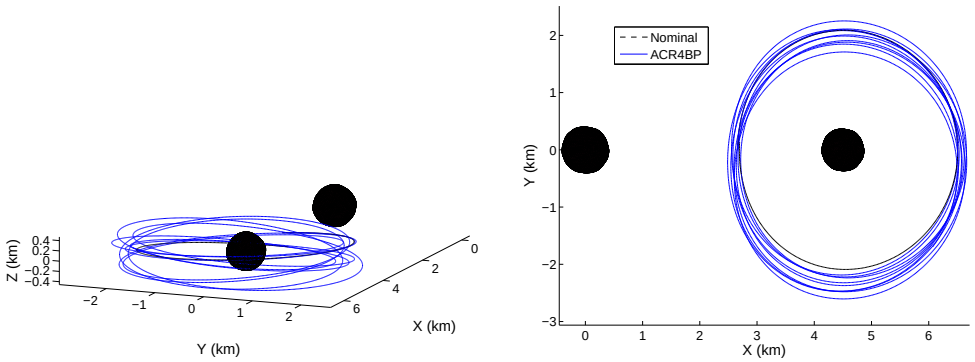

(a) 3D view (b) (x, y) projection

Figure 12. Sample stable DRO propagated in the RC4BP: mass ratio $\mu = 0.4$

SRP regime: terminator orbit Terminator orbits are constructed assuming that the spacecraft is orbiting a single body in the presence of strong SRP. A sample stable terminator orbit with an initial semi-major axis approximately equal to 6 nondimensional units is selected to be propagated in the ACR4BP for a system with a mass ratio equal to 0.0162. On the zonal map, such initial conditions correspond to a SRP dominated region with a MSCR approximately equal to 70. The initial and perturbed trajectories appear in Figure 13(a) in black and blue, respectively. The perturbation from the irregular shape of the bodies and the existence of a secondary massive body are evident, however, the resulting trajectory retains characteristics similar to the originating terminator orbit, in particular, the orientation of the orbital plane. Also, the trajectory remains bounded for the duration of the simulation, that is, 10 revolutions of the initial orbit. Then, a similar simulation is completed for a stable terminator orbit with a smaller semi-major axis value, $a = 3.3$, and a binary system with mass ratio increased to 0.196. These initial conditions now correspond to a binary effect dominated regime with a MSCR approximately equal to 5, and as expected, the perturbed trajectory is rapidly disrupted, as evident in Figure 13(b).

Binary effect regime: P_1 LoPO Although the low-prograde P_1-centered family is constructed in a three-body model, the low altitude of these trajectories with respect to P_1 place this family in the J_2 dominated regime on a zonal map. To assess the stability of such orbits, a sample stable orbit for mass ratio equal to 0.15 and with a MSCR approximately equal to 3 is propagated in the ACR4BP with an oblate irregular shape model for P_1. Recall that the dynamical model also includes the SRP and solar tide. The perturbed trajectory, propagated for 10 revolutions, is illustrated in Figure 14(a), and appears bounded in the vicinity of the initial trajectory. Further, the apparent precession of the blue perturbed orbit relative to the initial black orbit reflects the J_2 perturbation, however, the trajectory appears stable over the duration of the simulation. The same simulation is repeated for a significantly increased value of the SRP acceleration, from $\beta = 5$ to $\beta = 100$, and the corresponding perturbed trajectory is displayed in Figure 14(b). The inflated SRP force contributed to a more chaotic trajectory and the behavior of the spacecraft for longer-term propagation is unpredictable. Although this particular simulation results in a bounded orbit, slightly different initial conditions may yield undesired outcomes, such as an impact on the primary, given the large variation from the nominal trajectory.

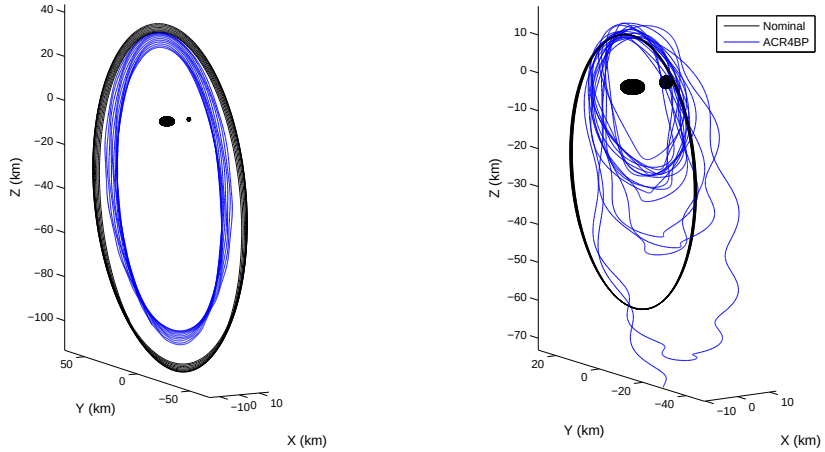

(a) mass ratio $\mu = 0.0162$, $a = 6$ (b) mass ratio $\mu = 0.196$, $a = 3.3$

Figure 13. Sample stable terminator orbits with $\beta = 5$ propagated in the ACR4BP

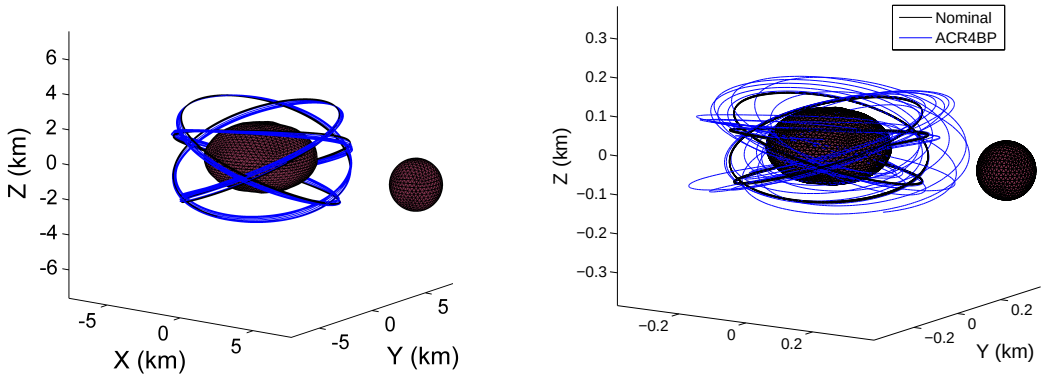

(a) $\beta = 5$ (b) $\beta = 100$

Figure 14. Sample stable P_1 LoPO propagated in the ACR4BP

SUMMARY AND CONCLUDING REMARKS

In an initial assessment of the perturbing effects that dominate the dynamics of a spacecraft in the vicinity of small irregular bodies, zonal maps are introduced. Such maps depict the dominating perturbations as a function of the orbit choice. Based on previous developments, classical perturbing effects are included, solar tide, SRP, and body oblateness. The analysis is extended to the binary effect, that is, the perturbation that arises from the existence of a binary system that includes a secondary body rather than a single body. The zonal maps are constructed from strength coefficients for the perturbations of interest, where these coefficients are derived exploiting LPEs. In addition, the binary effect strength coefficient leverages the third-body disturbing function. These mathematical tools rely on various assumptions and require validation. The strength coefficient for the additional

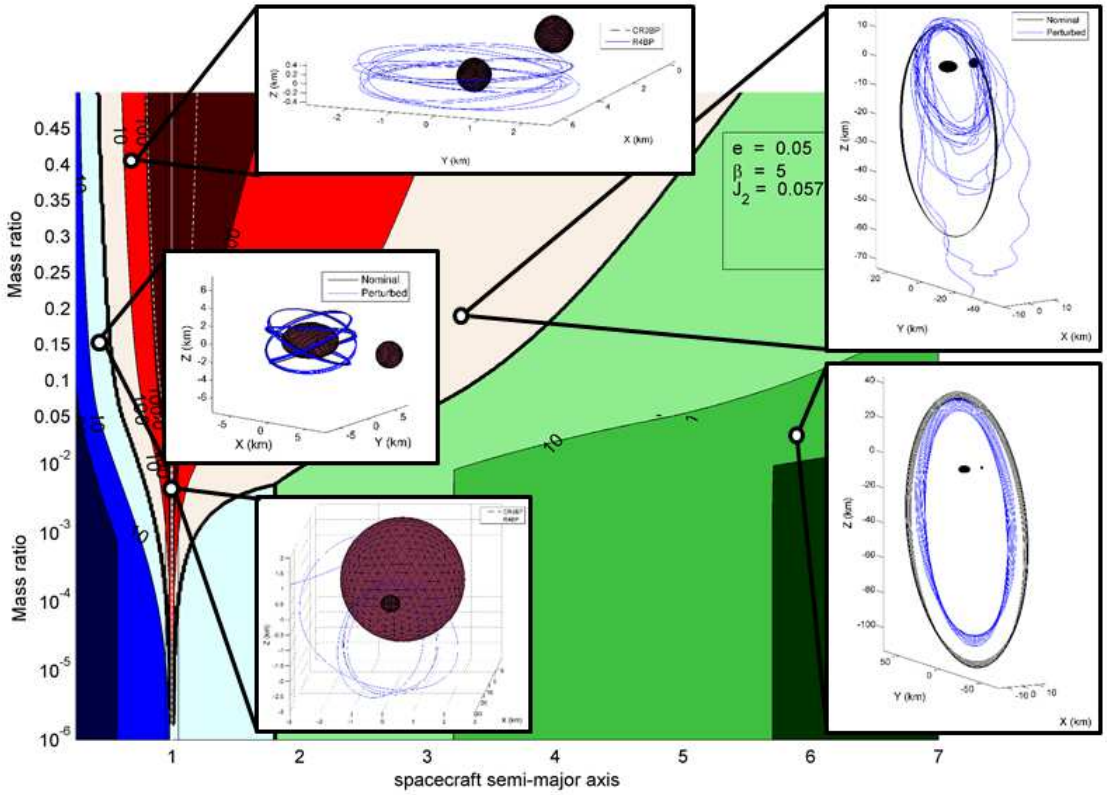

Figure 15. Summary of zonal map and sample trajectories

perturbation, the binary effect, is initially validated by comparing the LPE predictions with the numerical propagation of sample initial conditions. Then, the zonal maps are useful in selecting a type of orbit that is predicted to yield a stable ballistic motion under perturbations. Sample orbit types are considered as an initial application, including halos, terminators, DROs, and LoPOs, as summarized in Figure 15. Such an analysis may also aid in identifying which force ratios yield stable orbits for a given type. Future work involves further examination of the ballistic stability of sample types of orbits as a function of the ratio of the dominating strength coefficient to other perturbations.

ACKNOWLEDGMENT

Some of the work described in this paper was carried out at the Jet Propulsion Laboratory, California Institute of Technology, under a contract with the National Aeronautics and Space Administration.

REFERENCES

[1] K.-H. Glassmeier, H. Boehnhardt, D. Koschny, E. Khrt, and I. Richter, "The Rosetta Mission: Flying Towards the Origin of the Solar System," *Space Science Reviews*, Vol. 128, No. 1-4, 2007, pp. 1–21.

[2] http://osiris-rex.lpl.arizona.edu/. Last accessed 02-23-2013.

[3] J. L. Margot, M. Nolan, L. Benner, S. Ostro, R. Jurgens, J. Giorgini, M. Slade, and D. Campbell, "Binary asteroids in the near-earth object population," *Science*, Vol. 296, 2002, pp. 1445–1448.

[4] P. Michel, M. A. Barucci, A. Cheng, H. Böhnardt, J. R. Brucato, E. Dotto, P. Ehrenfreund, I. Franchi, S. F. Green, L. M. Lara, B. Marty, D. Koschny, and D. Agnolon, "MarcoPolo-R: Near Earth Asteroid

Sample Return Mission Selected for the Assessment Study Phase of the ESA program Cosmic Vision," *Acta Astronautica*.

[5] A. Cook, J. Bellerose, B. Rozitis, T. Yamaguchi, C. Mester, N. Murdoch, and F. Marchis, "Didymos Explorer: A Mission Concept for Visiting a Binary Asteroid," *AAS/Division for Planetary Sciences Meeting Abstracts #40*, Vol. 40 of *Bulletin of the American Astronomical Society*, Sept. 2008, p. 452.

[6] A. Cheng, A. Rivkin, C. Reed, O. Barnouin, Z. Fletcher, C. Ernst, A. Galvez, I. Carnelli, and P. Michel, "AIDA: Asteroid Impact & Deflection Assessment," *64th International Astronautical Congress*, Beijing, China, September 23-27 2013.

[7] D. J. Scheeres, "Satellite Dynamics About Asteroids," *Spaceflight Mechanics 1994, Part I, Advances in the Astronautical Sciences Series*, Vol. 87, San Diego, California, Univelt, 1994, pp. 275–292.

[8] K. Richter and H. Keller, "On the Stability of Dust Particle Orbits around Cometary Nuclei," *Icarus*, Vol. 114, No. 2, 1995, pp. 355 – 371.

[9] D. P. Hamilton and A. V. Krivov, "Circumplanetary Dust Dynamics: Effects of Solar Gravity, Radiation Pressure, Planetary Oblateness, and Electromagnetism," *Icarus*, Vol. 123, No. 2, 1996, pp. 503 – 523.

[10] C. D. Murray and S. F. Dermott, *Solar System Dynamics*. Cambridge University Press, 2000.

[11] F. Mignard and M. Henon, "About an unsuspected integrable problem," *Celestial Mechanics*, Vol. 33, No. 3, 1984, pp. 239–250.

[12] N. Bosanac, K. Howell, and E. Fischbach, "Stability of Orbits Near Large Mass Ratio Binary Systems," *2nd IAA Conference on Dynamics and Control of Space Systems*, Roma, Italy, March 24-26 2014.

[13] L. Chappaz and K. Howell, "Bounded Orbits near Binary Systems Comprised of Small Irregular Bodies," *AIAA/AAS Astrodynamics Specialist Conference*, San Diego, California, August 2014.

[14] D. J. Scheeres, S. B. Broschart, S. J. Ostro, and L. A. Benner, "The Dynamical Environment About Asteroid 25143 Itokawa, Target of the Hayabusa Mission," *AIAA/AAS Astrodynamics Specialist Conference and Exhibit*, Providence, Rhode Island, August 16-19, 2004.

[15] J. D. Hadjidemetriou, "Symmetric and Asymmetric Librations in Extrasolar Planetary Systems: A Global View," *Periodic, Quasi-Periodic and Chaotic Motions in Celestial Mechanics: Theory and Applications* (A. Celletti and S. Ferraz-Mello, eds.), pp. 225–244, Springer, 2006.

[16] D. W. Jordan and P. Smith, *Nonlinear Ordinary Differential Equations: An Introduction to Dynamical Systems*. New York: Oxford University Press Inc., 3rd ed., 1999.

[17] S. Broschart, G. Lantoine, and D. Grebow, "Quasi-terminator orbits near primitive bodies," *Celestial Mechanics and Dynamical Astronomy*, 2014, pp. 1–21.